

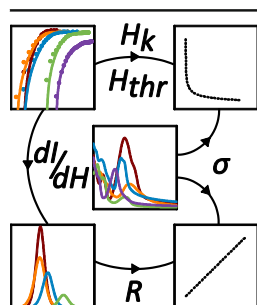
Matrix Optical Absorption in UV-MALDI MS

Kenneth N. Robinson,^{1,2} Rory T. Steven,¹ Josephine Bunch^{1,3}

¹National Center of Excellence in Mass Spectrometry Imaging (NiCE-MSI), National Physical Laboratory, Teddington, UK

²Advanced Materials and Healthcare Technologies Division, University of Nottingham, Nottingham, UK

³Department of Surgery and Cancer, Faculty of Medicine, Imperial College London, London, UK



Abstract. In ultraviolet matrix-assisted laser desorption/ionization mass spectrometry (UV-MALDI MS) matrix compound optical absorption governs the uptake of laser energy, which in turn has a strong influence on experimental results. Despite this, quantitative absorption measurements are lacking for most matrix compounds. Furthermore, despite the use of UV-MALDI MS to detect a vast range of compounds, investigations into the effects of laser energy have been primarily restricted to single classes of analytes. We report the absolute solid state absorption spectra of the matrix compounds α -cyano-4-hydroxycinnamic acid (CHCA), *para*-nitroaniline (PNA), 2-mercaptobenzothiazole (MBT), 2,5-dihydroxybenzoic acid (2,5-DHB), and 2,4,6-trihydroxyacetophenone (THAP). The desorption/ionization characteristics of

these matrix compounds with respect to laser fluence was investigated using mixed systems of matrix with either angiotensin II, PC(34:1) lipid standard, or haloperidol, acting as representatives for typical classes of analyte encountered in UV-MALDI MS. The first absolute solid phase spectra for PNA, MBT, and THAP are reported; additionally, inconsistencies between previously published spectra for CHCA are resolved. In light of these findings, suggestions are made for experimental optimization with regards to matrix and laser wavelength selection. The relationship between matrix optical cross-section and wavelength-dependant threshold fluence, fluence of maximum ion yield, and R , a new descriptor for the change in ion intensity with fluence, are described. A matrix cross-section of $1.3 \times 10^{-17} \text{ cm}^{-2}$ was identified as a potential minimum for desorption/ionization of analytes.

Keywords: UV-MALDI, MALDI, Matrix, Wavelength, Absorption, Fluence

Received: 4 August 2017/Revised: 31 October 2017/Accepted: 1 November 2017/Published Online: 29 November 2017

Introduction

Ultraviolet matrix-assisted laser desorption/ionization (UV-MALDI) is a surface sampling ionization technique used for analysis of a wide range of molecules, typically pharmaceuticals, biomolecules, and polymers [1–3], via mass spectrometry (MS). This is achieved through the application of a chemical additive, termed a matrix, to a sample. Upon laser irradiation, the matrix absorbs the laser energy, promoting desorption and ionization of analytes from the sample into the gas phase for subsequent analysis by the mass spectrometer. Due to its amenability to spatially selective sampling, UV-

MALDI-MS is also a widely employed modality for mass spectrometry imaging (MSI) applications [1, 4–6].

There remains much debate about ion formation mechanisms in UV-MALDI MS, with the principal proposed models all considering optical absorption one of the key matrix physicochemical properties involved in ion formation and desorption. The coupled physical and chemical dynamics (CPCD) [7–9] and Lucky Survivor (LS) [10–12] models both include excitonic energy pooling mechanisms within the matrix as pathways to ionization, which are governed by optical absorption. In the thermal proton transfer (TPT) model [13–15], while a different pathway for ionization is proposed, absorption remains important as it provides the means by which the matrix is heated to the necessary temperatures for ionization to occur.

The interplay between matrix optical absorption, laser wavelength, and energy strongly determines UV-MALDI MS performance and, consequently, have been the subject of a number of studies seeking to determine their relative influences. An early study by Allwood et al. compared matrix solid

Electronic supplementary material The online version of this article (<https://doi.org/10.1007/s13361-017-1843-4>) contains supplementary material, which is available to authorized users.

Correspondence to: Josephine Bunch; e-mail: Josephine.bunch@npl.co.uk

phase absorption coefficient (α) with qualitative assessments of matrix performance [16], showing a correlation between higher α and better performance [17]. Similar findings were reported with a range of DHB isomers at five laser wavelengths, with increased matrix adduct formation and analyte mass peak broadening also observed as a consequence of shorter wavelengths [18]. Chen et al. [19] investigated generation of polypeptide ions with the matrix compounds α -cyano-4-hydroxycinnamic acid (CHCA), sinapinic acid (SA), and β -indole acrylic acid across a range of near UV (NUV) wavelengths, finding that polypeptide ions were only detectable where the matrix α was $>6 \times 10^4 \text{ cm}^{-1}$, and when the average absorbed energy per volume in the surface layer of the matrix exceeded 8 kJ cm^{-3} . The wavelength and fluence dependency of ion intensity and ion yield, and their relationship to matrix solid phase absorption profiles, were investigated in a pair of recent studies by Soltwisch et al. [20, 21], with the highest analyte ion signals and optimal ion yields for both the total ion current (TIC) and analyte observed around the matrix absorption maxima. A very recent study from the same group expanded these experiments to additional matrix compounds and analytes [22].

Quantitative measurements of matrix optical absorption provide important data for fundamental studies of UV-MALDI MS. Usually such measurements are acquired from solutions [23–29], although this approach is potentially problematic as typically UV-MALDI matrix compounds are solids. Extensive differences between solution and solid phase spectra have been reported for UV-MALDI matrix compounds; typically these include a broadening and bathochromic shift of the absorption bands [17, 18, 20, 21, 30–32]; the appearance of new absorption bands has also been observed, e.g., CHCA and Coumarin 120 [17].

Many reported solid phase spectra have been recorded using spectrophotometers operating with diffuse reflection geometry. Unfortunately these measurements can only show the relative changes in absorption across wavelengths for given a sample [20, 21, 32], limiting comparison between different matrix compounds. To date, quantitative solid phase data have been reported for 11 matrix compounds [17, 31, 33], of which only 2,5-dihydroxybenzoic acid (2,5-DHB), SA, and CHCA remain widely used today. It is therefore beneficial to expand such measurements to include other matrix compounds used in contemporary UV-MALDI analyses, supporting refinement of ionization mechanism theories and helping to inform matrix selection in general experimentation.

Laser fluence, defined as the light energy delivered per unit area, has been identified as the primary laser parameter relevant to UV-MALDI MS. Generally it is observed that increasing fluence beyond the point at which ions are first detected, referred to as the threshold fluence, will result in rapidly rising ion intensity. Eventually with further increased fluence the ion signal will plateau through a combination of factors, including: fragmentation, photochemical effects, detector saturation, and complete ablation of the irradiated region. Threshold fluences in UV-MALDI MS vary considerably, ranging from ~ 10 –5000

J m^{-2} in dependence on focal spot size, laser wavelength, and matrix employed [34]. The matrix employed has a large impact on threshold fluences, which have been shown to correlate with the absorptive properties of the matrix [21]. Traditionally the relationship between fluence (H) and ion intensity (I) in UV-MALDI MS has been characterized via the function $H \propto I^m$ [34]. The exponent m is a fitting factor that describes the increase of ion intensity. Values for m vary considerably within the literature [34], and are strongly dependent on the matrix employed [35] and laser spot size [36, 37].

Recently a new function (Equation 1) was proposed that takes into account the saturation of the ion intensity signal at high fluences [21, 38].

$$I = \hat{I} \frac{(H - H_{thr})^m}{(H_k - H_{thr})^m + (H - H_{thr})^m} \quad (1)$$

This function makes use of three additional fitting factors as approximations for important characteristics of the ion intensity curve. H_{thr} describes the threshold fluence and \hat{I} the maximum ion intensity of the curve. The H_k parameter corresponds to the fluence at which the highest ion yield, and thus experimental sensitivity, may be obtained [21]; m in Equation 1 retains a similar function to that in the $H \propto I^m$ relationship, but is typically a factor of 0.75 smaller due to the influence of the other parameters [21].

In many previous fluence studies in UV-MALDI MS the analytes studied are, by and large, confined to a small range of peptides and proteins. A few investigations into laser energy effects have made use of different classes of analyte [22, 39, 40], although few have measured laser fluence [22, 41]. A systematic study of the relationship between laser fluence and detected ion intensity in UV-MALDI MS across a range of analyte classes and matrix compounds is therefore of clear interest.

In this study, quantitative solid phase optical absorption measurements of five common UV-MALDI matrix compounds were carried out. Experimentally measured densities for each of the studied matrix compound are also reported. MS data for the matrix compounds with three analytes were collected over a range of laser fluences to establish the relationship between matrix optical absorption, laser fluence, and detected ion intensity in UV-MALDI MS. The matrix compounds CHCA, *para*-nitroaniline (PNA), 2,5-DHB, 2-mercaptobenzothiazole (MBT), and 2,4,6-trihydroxyacetophenone (THAP) were selected for characterization. For the MS experiments, haloperidol, a common antipsychotic drug previously used in UV-MALDI MS studies [42, 43], angiotensin II, a small peptide hormone used in many UV-MALDI MS studies, and PC(16:0-18:1), referred to in this work as PC (34:1), a phosphatidylcholine lipid prevalent in cell membranes and widely used in many biophysical experiments, serve as representatives of common analyte classes encountered in UV-MALDI MS. Selection of these analytes also ensures a range of molar masses, log P and pKa values are included, as these have been reported as important properties

in UV MALDI MS [44, 45]. We make use of the recently published function describing the ion intensity fluence relationship [21] to probe various UV-MALDI MS experimental features; further treatment of the function is carried out enable extraction of additional information.

UV MALDI MS is a complex multi-step process where many factors can play a role in determining the final results, with energy absorption by the matrix, along with its photo-emissive, thermo-physical properties and gas phase chemistry considered critical to the desorption and ionization of analytes. Here we discuss the influence matrix absorption has on the ion intensity fluence relationship.

Materials

CHCA, PNA, MBT, THAP, haloperidol (375.9 g mol^{-1}), angiotensin II human ($1045.2 \text{ g mol}^{-1}$), and acetonitrile (ACN) were purchased from Sigma Aldrich (Gillingham, UK). 2,5-DHB was purchased from Alfa Aesar (Heysham, UK). PC(34:1) lipid standard (760.1 g mol^{-1}) was purchased from Avanti Polar Lipids (Alabaster, AL, USA). HPLC grade methanol (MeOH) was purchased from Fisher Scientific (Loughborough, UK). Unless stated otherwise, all water was deionised ($\rho = 15 \text{ M}\Omega\text{cm}^{-1}$) and generated using an Elga Purelab system (Elga, High Wycombe, UK). Stainless steel MALDI target plates were purchased from Sciex (Warrington, UK); $25 \text{ mm} \times 25 \text{ mm}$ quartz substrates were purchased from Agar Scientific (Stansted, UK). Quartz cuvettes (path length = 10 mm) were purchased from Hellma (Southend on Sea, UK). Silicon wafer (110, 20 nm SiO_2) was obtained from University Wafer (Boston, MA, USA)

Methods

UV-Vis Spectroscopy of UV-MALDI Matrix Compounds

Matrix thin films were deposited on quartz substrates using an Auto 306 Thermal Evaporator (Edwards, Eastbourne, UK) under intermediate vacuum conditions ($\sim 10^{-4}$ mbar). Silicon wafers ($10 \text{ mm} \times 10 \text{ mm}$) were simultaneously coated for deposited film thickness determination measurements. Both substrates were attached to a chilled ($\sim 5^\circ\text{C}$) block of copper with thermal conductive tape (3M, Bracknell, UK) to ensure deposition of the matrix compounds.

All absorption spectra were acquired using a UV-Vis spectrophotometer (Lambda 850, Perkin Elmer, Seer Green, UK). Solid phase absorption measurements were obtained from three different positions on the matrix thin films to account for any macroscopic variations in film thickness. Inclusion of another quartz substrate in the reference beam of the instrument meant that losses from reflection were primarily a result of differences in refractive index (n) between the matrix and substrate. From calculations using n values for cinnamaldehyde [46] and nitrobenzene [47] acting as analogues of the matrix compounds, we

estimate reflection losses (at normal incidence) to be no greater than 3%. Scattering effects were assumed to be negligible because of the high transparency and uniformity of the matrix films produced. Solution phase measurements were taken from 10 mmol L^{-1} solutions of matrix compound in MeOH; $700 \mu\text{L}$ of matrix solution was pipetted into a quartz cuvette for analysis. Another quartz cuvette filled with pure MeOH was used in the reference beam on the instrument.

Matrix Film Thickness Measurement

Deposited matrix film thickness was determined by atomic force microscopy (AFM: Cypher S, Asylum Research, High Wycombe, UK) measurements of the co-deposited Si wafers samples (Supplementary Figure S1). A pair of fine-tipped tweezers were used to manually score the films. AFM measurements were taken at four points along the scratches, and typically extended $20 \mu\text{m}$ from the edge of the trench to ensure that any material ploughing effects did not affect the height measurement. The substrate flatness in the AFM images served as a quality check that no damage had occurred and that the matrix layer had been effectively removed.

Matrix Compound Density

Matrix compound density was determined using an AccuPyc 1340 gas pycnometer (Micromeritics, Hexton, UK). Samples of matrix powder were placed in a desiccator for 5 days prior to the analysis to minimize the effects of absorbed atmospheric water on the measurements. A minimum of five measurements were performed at 21°C , using helium as the displacement medium.

UV-MALDI MS

UV-MALDI MS data were collected over a mass range of 50–1100 m/z in positive mode using a QSTAR XL QqTOF mass spectrometer fitted with a oMALDI2 source (Sciex, Warrington, UK), coupled via $100 \mu\text{m}$ round optical fiber (Fiberguide Industries, Stirling, NJ, USA) to a 355 nm Nd:YAG DPPS laser (FQS-100-1-Y-355, Elforlight, Daventry, UK), operating at 1 kHz with a pulse width of <4 ns. The laser was triggered with a square wave signal by a function generator (TG2000 20 MHz DDS, TTi, High Wycombe, UK). A shutter system, previously described by Steven et al. [48], was used to aid pulse energy stability during experiments. Data collection was controlled via the Analyst QS 1.1 and oMALDI server 5.1 software packages (Sciex, Warrington, UK).

Laser Fluence Measurement

Pulse energy was monitored by sampling the beam with a partially reflecting mirror (BSF-10-UV, Thorlabs, Exeter, UK) prior to entry into the fiber, and diverting it towards a photodiode sensor (PD10-C, Ophir Photonics, Darmstadt, Germany). Delivered pulse energy was determined through calibration to post experiment end of fiber measurements, corrected for known losses (13%) from the delivery optics of the instrument. The laser incidence angle was approximately

65°, forming an elliptical spot $111 \mu\text{m} \times 235 \mu\text{m}$ at the sample, as determined via the fluorometric method [49] from CHCA thin films using ImageJ [50]. Variation in delivered laser fluence was achieved via a Brewster angle variable attenuator (Watt Pilot, Altechna, Vilnius, Lithuania).

Laser Fluence Variation Experiments

Combinations of each matrix compound and analyte were dissolved in 80:20 MeOH:H₂O at 10,000:1 molar ratio, and deposited onto stainless steel MALDI imaging plates using a pneumatic sprayer (TM Sprayer, HTX Imaging, Chapel Hill, NC, USA). The nominal deposited surface concentrations of the matrix and analyte were $9.55 \times 10^{-9} \text{ mol mm}^{-2}$ and $9.55 \times 10^{-13} \text{ mol mm}^{-2}$, respectively. UV-MALDI MS data were collected as individual raster lines in continuous raster mode over a range of laser fluences (5 to 360 J m^{-2}) at 0.2 mm s^{-1} raster speed, with a horizontal pixel size of $200 \mu\text{m}$, resulting in 1000 laser shots per acquired spectrum. The raster lines were vertically separated by $800 \mu\text{m}$ to ensure no oversampling of previous raster lines.

Data Analysis

Unless stated otherwise, all data were processed in MATLAB (R2016b, MathWorks, Cambridge, UK). AFM data were processed in SPIP (v 6.6.3, Image Metrology, Hørsholm, Denmark), film thicknesses were determined via histogram analysis using the Step Height function. MS data were converted to .mzML using AB MS Data Converter (v 1.3, Sciex, Warrington, UK) and then into .imzML using imzMLConverter [51], and imported into MATLAB using SpectralAnalysis [52] for further processing and analysis. Spectral data underwent a zero filling process before peak intensities, taken as the integrated area at full width half maximum (FWHM), were extracted. Data fitting was carried out in OriginPro 2016 (OriginLab, Stoke Mandeville, UK) using the Levenberg-Marquardt algorithm.

Results

Matrix Compound Solid Phase Optical Absorption

For a direct comparison of optical absorption properties between matrix compounds, it is necessary to obtain quantitative absorption measurements. The most commonly encountered metrics for this property in solids are α and optical cross section (σ). These metrics are measures of different aspects of absorption, with α describing the absorption per unit volume and σ the absorption per molecule. They can be calculated using Equations 2 and 3.

$$\alpha = \frac{A_e}{l} \quad (2)$$

$$\sigma = \frac{\alpha}{n} \quad (3)$$

where A_e = Napierian absorption, l = path length, and n = number density. l was determined via AFM measurements of scratches in the matrix thin films, showing that the deposited matrix films ranged from 34 to 152 nm in thickness (Supplementary Figure S1a). n was calculated from measured densities for the studied matrix compounds (Table 1). To our knowledge, these are the first directly measured density values for CHCA, 2,5-DHB, and THAP, and should supplement future UV-MALDI fundamentals studies.

Quantitative data on matrix optical properties, from solid state measurements most applicable to UV-MALDI MS experimental conditions, are essential for investigating the role of the matrix in ion formation. Solid phase σ data for the matrices used in this study, with the corresponding solution phase data for comparison, are shown in Figure 1. The solid phase data plotted as absorption coefficient spectra can be found in Supplementary Figure S2.

To our knowledge, these spectra are the first quantitative solid phase optical absorption data for PNA, MBT, and THAP reported in literature. As previously observed with UV-MALDI matrix compounds [18, 20, 21, 31, 33], the solid phase spectra showed noticeable differences compared with spectra obtained from solution, with broader absorption bands observed for all matrix compounds (Figure 1). Absorption band broadening in organic molecular solids is characteristic of the existence of excitonic bands within the crystal structure, which arise because of the interaction of photo-excited states with neighboring molecules and with the crystal lattice structure as a whole [53]. This absorption band broadening also accounts for the hypochromic shift of solid phase spectra observed for all the matrix compounds, attributable to the population of excited states being divided among a greater number of energy levels.

Relative to the data collected from solution, a bathochromic shift in the absorption spectra of up to 30 nm was observed for the solid phase (Figure 1). This effect is termed the “solvent shift” and arises from intermolecular interactions, such as Van der Waals bonding [53]. Hypsochromic shifts in absorption spectra can arise from solvent dipole–dipole interactions and H-bonding on molecular electronic transition energies [54]. The solvent used here was methanol, a polar protic solvent; therefore the observed bathochromic shift in the solid phase spectra is likely the result of a relative reduction in dipole–dipole interactions and H-bonding, and increase in Van der Waals bonding.

New absorption bands were observed for CHCA, MBT, and PNA and to a lesser extent 2,5-DHB (Figure 1). In molecular solids this behavior is characteristic of Davydov splitting, whereby interactions between molecules within the crystal unit cell leads to a splitting of a given molecular electronic transition into n bands, where n is the number of differently oriented molecules within the unit cell [53]. With the exception of THAP, Davydov splitting has been previously reported for all the matrix compounds studied here [30, 33, 55, 56].

For practical use of these qualitative optical absorption data, it is convenient to present the values at wavelengths of common UV-MALDI MS lasers (Table 1). Additionally, in light of the

Table 1. Densities and Solid State α and σ of the Selected UV-MALDI Matrix Compounds

Matrix compound	Density (g cm ⁻³)	NUV λ_{\max} (nm)	α (10 ⁵ cm ⁻¹)			σ (10 ⁻¹⁷ cm ⁻²)		
			α_{337}	α_{355}	$\alpha_{\text{NUV } \lambda_{\max}}$	σ_{337}	σ_{355}	$\sigma_{\text{NUV } \lambda_{\max}}$
CHCA	1.44	350	3.82 ± 0.46	4.12 ± 0.51	4.18 ± 0.51	8.31 ± 1.00	8.98 ± 1.17	9.09 ± 1.11
PNA	1.43	374	1.21 ± 0.15	1.68 ± 0.20	1.83 ± 0.22	1.94 ± 0.23	2.70 ± 0.32	2.95 ± 0.36
MBT	1.51	333	3.25 ± 0.90	2.60 ± 0.73	3.30 ± 0.91	5.96 ± 1.65	4.76 ± 1.34	6.06 ± 1.68
2,5-DHB	1.57	351	0.81 ± 0.14	0.87 ± 0.15	0.91 ± 0.15	1.32 ± 0.23	1.42 ± 0.24	1.43 ± 0.24
THAP	1.48	304	1.05 ± 0.19	0.74 ± 0.13	2.54 ± 0.45	1.98 ± 0.35	1.40 ± 0.25	4.80 ± 0.85

Values corresponding to the common laser wavelengths employed in UV-MALDI (337 and 355 nm) and the NUV λ_{\max} are reported, as well as the position of the NUV λ_{\max} . The expanded uncertainty ($k = 2$) is reported, for density measurements these were typically <0.001 g cm⁻³ so are not included

demonstration of tuneable-wavelength laser systems for UV-MALDI MS [19–21, 32] and previous recommendations for

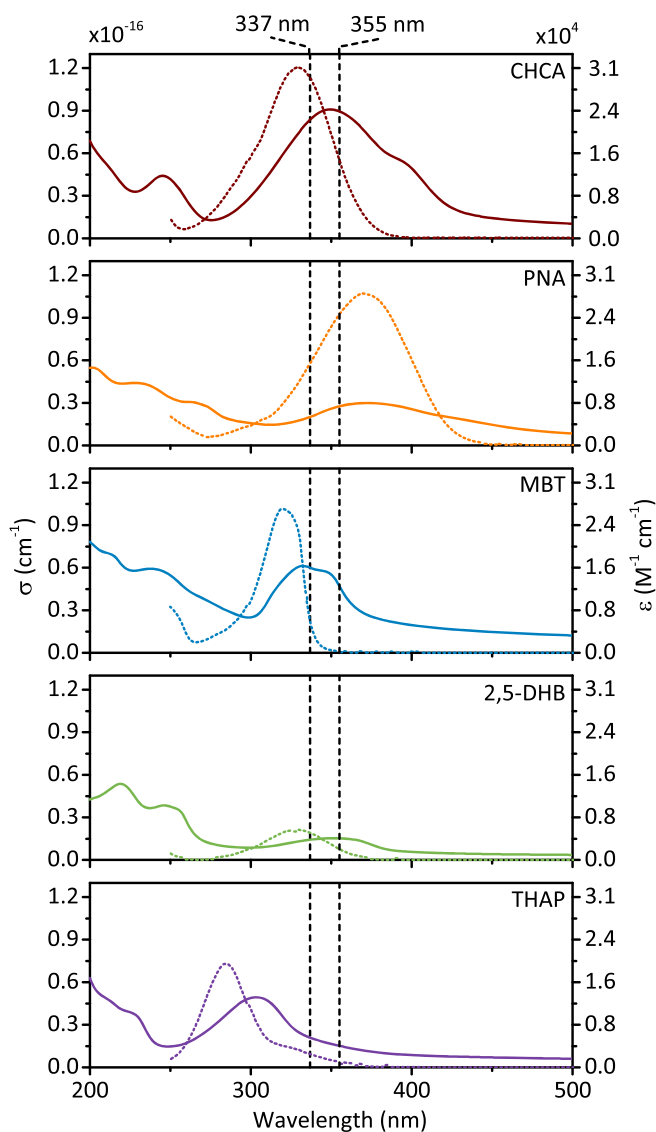


Figure 1. Solid phase optical cross section (σ) spectra for the five studied UV-MALDI matrix compounds, as measured from sublimed thin films. Dotted lines are the solution phase absorption spectra of the corresponding matrix (10 mmol L⁻¹ in MeOH). The right axis shows the equivalent molar extinction coefficient (ϵ) scale. Dashed vertical lines mark the operating wavelengths of common UV-MALDI lasers

optimal wavelength ranges [18], the λ_{\max} of the matrix compounds in the near-UV region (300–400 nm) are also included.

For the matrix compounds studied α values were typically of the order of 10⁵ cm⁻¹, and σ of the order of 10⁻¹⁷ cm⁻²; α values are of the same order as those reported by Allwood et al., who measured an α_{337} of 2.18×10^5 cm⁻¹ and 0.80×10^5 cm⁻¹ for CHCA and 2,5-DHB sublimed thin films respectively [17]. While our findings for 2,5-DHB are in good agreement with their data, their α_{337} for CHCA is significantly smaller (43%) than our measurements. It should be noted that the observed NUV λ_{\max} for CHCA in that work occurred at ~ 370 nm, noticeably different from that found here (Table 1). Back calculations of their data yields a CHCA $\alpha_{\text{NUV } \lambda_{\max}}$ only 13% smaller than our finding. This suggests that the differences in NUV λ_{\max} position is likely responsible for the discrepancy between in CHCA α_{337} . The reason for this difference is not known, although other reported NUV λ_{\max} for CHCA are in agreement with the findings presented here [20].

The molar attenuation coefficient (ϵ) for 2,5-DHB spin coated films has been previously reported by Heise and Yeung as 2.80×10^3 M⁻¹cm⁻¹ at 337 nm [31]; this corresponds to a σ_{337} of 1.07×10^{-17} cm⁻² and is 19% smaller than the value obtained here. The difference between the two results may be due to the alternate methods of deposition employed, or the film thickness and matrix compound density were not directly measured in that work. Similarly, σ values reported by Allwood et al. for CHCA and 2,5-DHB used an assumed matrix density of 1.1 g cm⁻³; recalculation using the new density values reported here yields $\sigma_{\text{NUV } \lambda_{\max}}$ that are 13% and 3% smaller than our measurements for CHCA and 2,5-DHB, respectively, in good agreement with our findings.

Comparison of the σ values at the wavelength of the laser used in this study (355 nm) showed that CHCA was by far the most strongly absorbing matrix (Table 1). The σ_{355} of the remaining matrix compounds, MBT, PNA 2,5-DHB, and THAP, were 53%, 30%, 16%, and 16% of the CHCA σ_{355} , respectively. The σ_{337} and σ_{355} values showed a correlation with widely used characterizations of the matrix compounds with relation to analyte fragmentation, with the traditionally “hot” matrix compound CHCA [57] having the largest σ and “cold” matrix compounds 2,5-DHB and THAP [57, 58] demonstrating the smallest.

Ion yields within UV-MALDI MS have been reported as highest around the λ_{\max} of the matrix employed [20, 21]; thus

the solid phase spectra presented here (Figure 1) can be used to identify optimal laser wavelengths for UV-MALDI MS experimentation with these matrix compounds. Comparison of the σ_{337} , σ_{355} , and $\sigma_{\text{NUV } \lambda_{\text{max}}}$ values (Table 1.) shows that most of the compounds are already well suited to standard UV-MALDI MS lasers. The one exception was THAP, which has σ_{337} and σ_{355} only 41% and 29% that of its $\sigma_{\text{NUV } \lambda_{\text{max}}}$. The use of XeCl excimer (308 nm) lasers may be beneficial for this matrix, or alternatively, wavelength-tuneable lasers, previously demonstrated in UV-MALDI MS [19–21, 32], enabling direct matching of laser wavelength to the matrix λ_{max} .

Previous studies used qualitative solution measurements as representative of solid phase data [17, 18]. Here the ratio of $\sigma_{\text{NUV } \lambda_{\text{max}}}$ in solid phase to that in solution ranged from 1.4 for CHCA to 3.3 for THAP, suggesting estimations of solid phase absorption from data acquired from solutions are reliable to within a factor of 3. This represented a reduction in the accuracy of such an approach, previously around a factor of 2 [17], and demonstrates that solution absorption measurements should be used with caution for estimating matrix solid phase absorption.

Desorption/Ionization as a Function of Laser Fluence for Different Matrix Compounds and Analytes

A complex interaction of factors is believed to contribute to ionization and desorption in UV-MALDI MS, reflecting the multistep nature of the technique. Each step of the UV-MALDI process will have its own requirements with regards to matrix properties, with absorption and photoemission, thermo-physical properties and gas phase chemistry among those considered critical to the desorption and ionisation of analytes. To investigate the influence of matrix optical absorption on UV-MALDI MS results, data were acquired at a range of laser fluences, with a range of analytes (Figure 2). The compounds selected here were haloperidol, angiotensin II, and PC (34:1). The use of multiple analytes provides the opportunity to probe differences that can arise in UV-MALDI MS analyses, particularly imaging experiments where multiple classes of analyte are being ionized. It was also useful to control other experimental parameters, such as matrix:analyte molar ratio, as these are rarely controlled in fluence variation experiments. The recently proposed sigmoidal function (Equation 1) [21] was used to fit our data, allowing more experimentally pertinent features of the fluence-ion intensity data to be described.

In line with previous observations [34], threshold fluences for the analytes ($H_{\text{thr } A}$) were strongly matrix-dependent, with the matrix compounds falling into two distinct groups (Figure 2). With $H_{\text{thr } A}$ for 2,5-DHB and THAP much higher than those found for CHCA, PNA, and MBT, this relative ordering is broadly in line with previous observations [21, 35–37, 59–61]. Due to the strong influence laser spot size has on H_{thr} [36, 37, 59, 61], direct comparison with reported values is difficult, although previous work from our lab reported H_{thr} for CHCA in good agreement with the values shown here [41]. The ordering of $H_{\text{thr } A}$ by matrix compound generally reflects the relative

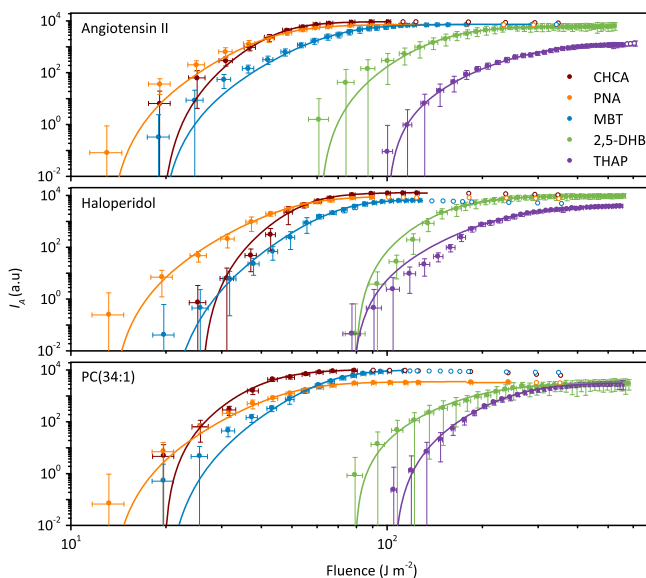


Figure 2. Analyte $[M+H]^+$ intensity (I_A) with varying laser fluence for the studied matrix analyte mixed systems. Data points are the mean I_A taken from 45 spectra, x and y error bars show the expanded uncertainty ($k = 2$). Solid line represents fitting of the data of Equation 1, open data points signify the onset of reduction in I_A due to fragmentation, this regime is not modeled by the equation and thus excluded in the fitting process

absorptions at the wavelength of the laser used (Table 1), with the exception of PNA, which deviated from the trend. This is in agreement with previous findings that H_{thr} has some correlation with the absorption spectrum of the matrix [21], although as UV-MALDI is a complex process, other variables are expected to contribute to the observed result.

$H_{\text{thr } A}$ appears to exhibit a small dependence on the analyte in question as well as the matrix used in some instances (Supplementary Figure S3); for example haloperidol demonstrated a $H_{\text{thr } A}$ 30% higher for CHCA but 30% lower for THAP compared with the other analytes. Matrix crystal morphology has been previously reported as having an effect on threshold fluences in UV-MALDI MS [62]. Inspection of the samples under a microscope showed differences in the morphology of deposited CHCA when haloperidol was the analyte (data not shown), potentially explaining the different $H_{\text{thr } A}$. On the other hand, both THAP appeared visually identical for all the analytes. $H_{\text{thr } A}$ has been previously suggested as dependent on analyte molecular mass [44]. Whilst no trend of this nature was evident in our data, the fact that the mass range of the analytes investigated here (376–1046 Da) was much smaller than that examined in that study (5.7–66 kDa) may explain this discrepancy.

Using the previously measured absorption coefficient data for the matrix compounds, the energy per unit volume (E_V) in the surface layers of the samples upon irradiation, ignoring losses due to reflection, can be calculated via Equation 4 [34]

$$E_V = \alpha H_0 \quad (4)$$

where H_0 = incident laser fluence.

E_V at the observed threshold fluence ranged from 0.2 to 1 kJ cm⁻³ for the matrix compounds studied, which is significantly lower than the 8 kJ cm⁻³ determined by Chen et al. [19], although Dreisewerd suggests [34] this is anomalously high and most reported values are in the order of 1 kJ cm⁻³, in agreement with our findings. Typical energy densities at the observed threshold fluences were 43 kJ mol⁻¹, 128 kJ mol⁻¹, 166 kJ mol⁻¹, 188 kJ mol⁻¹, and 215 kJ mol⁻¹ for PNA, MBT, 2,5-DHB, THAP, and CHCA, respectively. While these values represent approximately the amount of energy absorbed by the matrix compounds at the observed threshold fluence, it should be noted that they will not fully describe the energy available for UV-MALDI desorption/ionisation processes due to the existence of other energy decay mechanisms. Fluorescence in particular has been reported to account for a significant proportion of absorbed energy in some matrix compounds [63], although there is still large uncertainty in the exact values [64]. The large difference in energy densities between matrix compounds with similar H_{thr} , CHCA, MBT, and PNA is striking, revealing the influence of additional matrix compound physicochemical properties. Sublimation enthalpies have been reported for some of the matrices studied here [65, 66], although, in agreement with previous investigations [65, 67], no correlation is observed. Similarly no correlation with matrix proton affinity could be found. Interestingly, a correlation with the melting point of the matrix is evident (Figure 3), which suggests that other thermodynamic properties may be playing a role. This may somewhat explain why PNA, a matrix known to readily sublime at room temperature in vacuum [68, 69], had a similar observed H_{thr} to CHCA despite having a significantly smaller σ_{355} . Further studies to characterize such properties are therefore clearly of interest.

H_k describes the inflection point of the ion intensity-fluence curve, and has been proposed as the optimal fluence for UV-MALDI analyses [21]. H_{kA} demonstrated a similar dependency on matrix as H_{thrA} (Figure 2). H_{kA} values for CHCA, PNA,

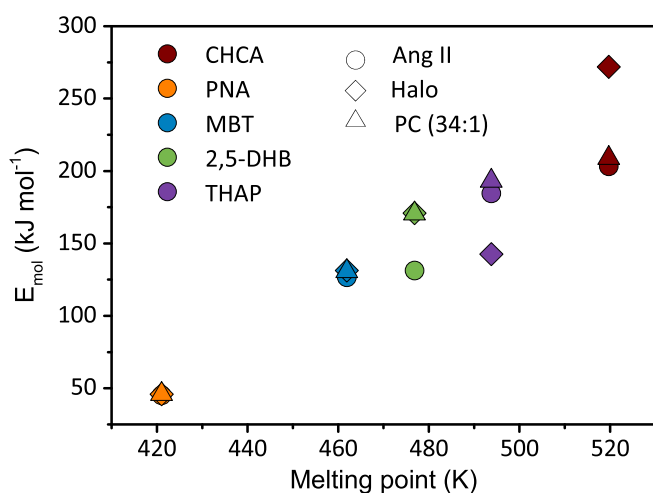


Figure 3. Calculated surface layer energy densities at observed threshold fluence for the studied matrix-analyte combinations, as a function of matrix melting point

MBT, 2,5-DHB, and THAP were approximately 50 J m⁻², 50 J m⁻², 73 J m⁻², 200 J m⁻², and 300 J m⁻², respectively, although the variance in data is large. H_{kA} was also somewhat analyte-dependent (Supplementary Figure S4). With CHCA, haloperidol resulted in a 20% higher H_{kA} compared to the other analytes. Both PNA and MBT showed relatively little variation arising from different analytes. With respect to the other analytes, PC34:1 demonstrated ~30% higher H_{kA} when 2,5-DHB was the matrix and angiotensin II ~10% higher with THAP. Overall, as with H_{thrA} , there was no discernible trend to the variation.

The maximum observed analyte $[M+H]^+$ intensity (\hat{I}_A) also varied considerably depending on the matrix compound used (Figure 2). For all the analytes studied, CHCA consistently produced the highest \hat{I}_A values, ranging from 4% to 30% higher than next highest \hat{I}_A . Owing to limitations in the accessible experimental fluence range, \hat{I}_A values for 2,5-DHB and THAP were obtained from projection of the fitting curve, and as such some caution should be taken with their interpretation.

\hat{I}_A also varied with analyte for a given matrix (Supplementary Figure S4). Haloperidol produced the highest \hat{I}_A for all the matrix compounds with the exception of MBT, ranging from 20% to 300% higher than the other analytes. As molar concentrations of matrix and analyte were constant for all experiments, these findings can be taken as approximately indicative of matrix ionization efficiency towards the individual analytes, under the conditions studied. With this in mind, it is clear that CHCA is the most efficient matrix for the analytes studied, and that with the exception of MBT, haloperidol was the most readily ionized of the analytes.

The parameter m has been previously described as matrix-dependent [21]; in this study values for m for the analyte ion intensity (m_A) was found to be typically lower for 2,5-DHB (2.7–3.4) and THAP (2.7–3.2), and larger for CHCA (3.4–4.2), PNA (3.8–4.0), and MBT (3.9–4.8), loosely reflecting the division observed in previously discussed properties such as σ_{355} and “hot” and “cold” matrices. The effect of analyte on m_A values was seemingly uncorrelated with known properties, with variation of the order of ± 1 .

The ion intensity-laser fluence relationship can be alternatively visualized by plotting derivatives of the ion intensity curves (Figure 4). This approach provides a more intuitive extraction and understanding of some experimental features and trends. The fluences at which both H_{thr} and \hat{I} occur are located at the two x-intercepts, and H_k can be easily identified as corresponding to the locations of the derivative curve maxima on the x-axis.

By taking the height of the derivative of Equation 1, it is possible to determine the maximum rate of change in ion intensity with laser fluence. This new metric, which we term R , can be thought of as a more intuitive alternative to the m parameter, which also describes the increase in ion intensity. As with m_A , the maximum rate of change in I_A (R_A) was influenced by matrix utilized (Figure 4), with CHCA producing the highest R_A (340–380) of all the

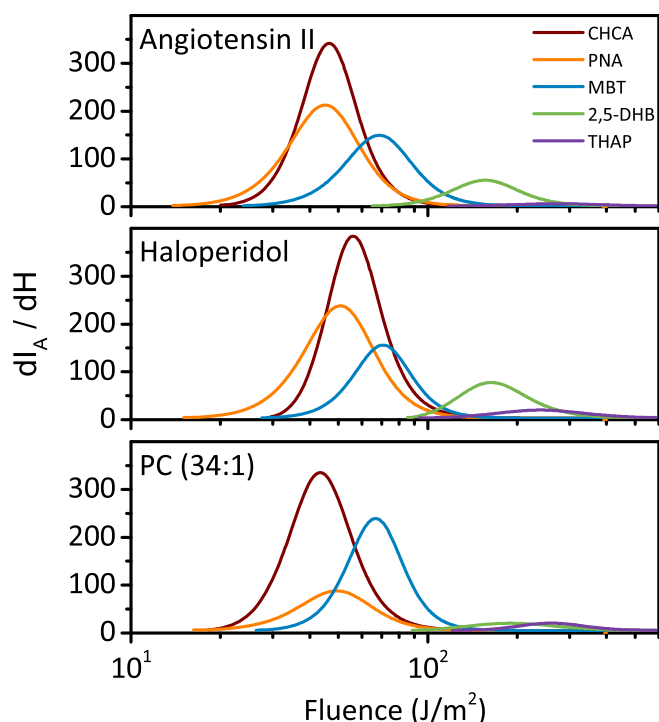


Figure 4. Derivative forms of the change in ion intensity with fluence produced by fitting of the data to Equation 1, for each of the matrix analyte combinations

matrix compounds, for all analytes. R_A values with PNA (84–235) and MBT (149–235) were approximately grouped together, while the lowest R_A values were obtained with 2,5-DHB (16–75) and THAP (5–17). The grouping of R_A is somewhat reflective of the matrix compound optical absorption, although the scatter in values for PNA and 2,5-DHB indicate other factors are having a strong influence. Unlike m_A there was a noticeable trend in R_A with respect to the analyte used (Figure 4), with haloperidol giving the largest R_A , for all matrix compounds with the exception of MBT.

Desorption/Ionization Characteristics as a Function of Matrix Optical Absorption

Defining the relationship between the various physicochemical properties of a matrix compound and its desorption/ionization characteristics is a long standing goal in UV-MALDI research. Such knowledge would benefit ionization mechanism investigations, but could also guide rational development of new matrix compounds for improving UV-MALDI MS analyses. Keeping in mind that optical absorption is only one of many properties that have been identified as critical in UV-MALDI MS, the matrix σ_{355} was compared with the parameters obtained from the fluence variation experiments, to further explore

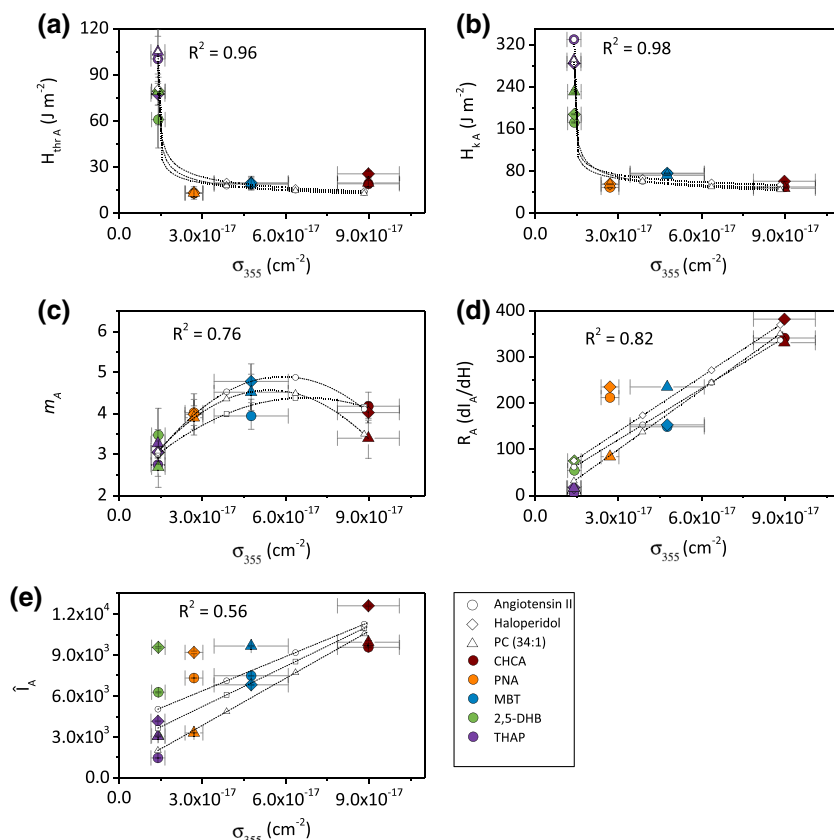


Figure 5. Relationship between matrix optical cross-section at 355 nm (σ_{355}) and the analyte ion intensity curve parameters (a) H_{thrA} (b) H_{kA} (c) m_A (d) R_A and (e) \hat{I}_A , for the 15 studied matrix analyte combinations. Error bars represent the expanded uncertainty ($k = 2$). Lines in the plots represent fitting of the data to (a) and (b) power, (c) second order polynomial, and (d) and (e) linear functions

the relationship between this specific matrix property and analyte desorption/ionization (Figure 5).

Both $H_{thr A}$ and $H_{k A}$ can be modeled with a power law relationship (Figure 5a and b) of the form

$$H_{(thr,K)} = n(\sigma - \sigma_{min})^{-p} \quad (5)$$

where n and p are fitting parameters; p for both $H_{thr A}$ and $H_{k A}$ had similar values, ranging from 0.26 to 0.44; n was slightly larger for $H_{k A}$ (2.0×10^{-5} to 3.1×10^{-3}) than $H_{thr A}$ (1.0×10^{-6} to 1.1×10^{-4}). Both parameters varied with analyte, although with no obvious correlation. σ_{min} , which describes the point on the x-axis where the curve tends to infinity, ranged from 1.28×10^{-17} to $1.39 \times 10^{-17} \text{ cm}^{-2}$, and appeared to scale inversely with analyte molecular mass. For the matrix compounds studied, this corresponds to an α of 6×10^4 to $8 \times 10^4 \text{ cm}^{-1}$, which is close to the $6 \times 10^4 \text{ cm}^{-1}$ observed by Chen et al. as the minimum α required for detection of analytes [19]. The wavelengths at which the α of CHCA and 2,5-DHB fall below this minimum also correspond closely to those observed by Soltwisch et al. at which significant drops in observed analyte ion intensities for these matrix compounds occurred [21]. Data for THAP from a recent work from the same group also showed signs of this effect [22]. σ_{min} could therefore, tentatively, be thought of as describing the minimum σ required for a compound to function as an effective matrix in UV-MALDI MS, although further studies with additional matrix compounds and laser wavelengths would be necessary to confirm this. From the relationship (Figure 5a and b) it can be seen that decreasing matrix cross-section below $2 \times 10^{-17} \text{ cm}^{-2}$ resulted in rapidly increasing $H_{thr A}$ and $H_{k A}$. Such information can be useful in guiding identification of novel matrix compounds, if for example one was seeking to create matrix compounds that are optimized for low fluences to minimize fragmentation or extend laser lifetimes.

Both m_A and \hat{I}_A showed only weak correlations to σ (Figure 5c and e). \hat{I}_A has been reported as wavelength-dependant [21] and therefore would be expected to show some relation to matrix σ ; the discrepancy may be due to the uncertainty in determining \hat{I}_A in this study. R_A showed a strong linear relationship with matrix σ (Figure 5d), highlighting another benefit of using this metric over m .

Conclusion

Quantitative solid phase optical absorption spectra were acquired for a selection of common UV-MALDI matrix compounds. These data were employed, in conjunction with MS experiments, using multiple analytes across a range of laser fluences, to investigate the influence of matrix optical absorption on desorption/ionization characteristics in UV-MALDI MS. We report the solid phase optical absorption and densities for the selected matrix compounds, most for the first time. While no significant alterations to current UV-MALDI ionization models are expected, incorporation of this new

physicochemical data presented here can improve the quality of theoretical predictions, as well as aid the extension of the existing models to a broader range of matrix compounds.

The desorption/ionization of analytes was found to be determined, in part, by matrix optical absorption, with the influence of other factors also apparent. Correlation of estimated threshold fluence energy densities within the matrix with melting point suggests further characterization of matrix compounds, such as thermo-physical or photo-emissive properties, could provide additional insight on energy uptake in UV-MALDI MS. The variances observed in the desorption/ionization characteristics of the different analytes has important implications with regards to experimental optimization. Careful consideration of matrix choice and laser energy is required, particularly in MSI studies where multiple analytes are being detected simultaneously, to ensure the validity of conclusions drawn from resulting data.

The alternative visualization of the ion intensity data provided useful information. In particular, enabling extraction of the R metric, displayed a stronger correlation with matrix σ , than the commonly employed m factor.

Finally, identified constraints on matrix σ required for detection of analyte ions, in line with previous findings [19], point to an aspect of ion generation in UV-MALDI MS that warrants investigation in future studies. Future work will seek to characterize additional physicochemical properties that influence desorption/ionization, which should further progress towards the realisation of a physicochemical underpinning for rational design and selection of new matrix compounds and help refine fundamental models, improving the capabilities of UV-MALDI MS and MSI.

Acknowledgments

The authors thank Stuart Davidson (NPL) for performing the density measurements, and the rest of the NiCE-MSI team, in particular Spencer Thomas, Alan Race, Adam Taylor, and Alex Dexter, as well as David Barratt (University of Nottingham) for helpful discussions and feedback on the manuscript. Funding for the work presented here was provided through the AIMS HIGHER project as part of the NPL strategic research program.

References

1. Greer, T., Sturm, R., Li, L.: Mass spectrometry imaging for drugs and metabolites. *J. Proteom.* **74**, 2617–2631 (2011)
2. Bonk, T., Humeny, A.: MALDI-TOF-MS analysis of protein and DNA. *Neuroscientis.* **7**, 6–12 (2001)
3. Li, L.: Overview of MS and MALDI MS for polymer analysis. In: MALDI mass spectrometry for synthetic polymer analysis. pp. 1–8. John Wiley & Sons, Inc., Hoboken (2009)
4. Amstalden van Hove, E.R., Smith, D.F., Heeren, R.M.A.: A concise review of mass spectrometry imaging. *J. Chromatogr. A* **1217**, 3946–3954 (2010)
5. Balluff, B., Schöne, C., Höfler, H., Walch, A.: MALDI imaging mass spectrometry for direct tissue analysis: technological advancements and recent applications. *Histochem. Cell Biol.* **136**, 227–244 (2011)

6. Castellino, S., Groseclose, M.R., Wagner, D.: MALDI imaging mass spectrometry: bridging biology and chemistry in drug development. *Bioanalysis*. **3**, 2427–2441 (2011)
7. Knochenmuss, R.: A quantitative model of ultraviolet matrix-assisted laser desorption/ionization. *J. Mass Spectrom.* **37**, 867–877 (2002)
8. Knochenmuss, R.: A quantitative model of ultraviolet matrix-assisted laser desorption/ionization including analyte ion generation. *Anal. Chem.* **75**, 2199–2207 (2003)
9. Knochenmuss, R.: The coupled chemical and physical dynamics model of MALDI. *Annu. Rev. Anal. Chem.* **9**, 365–385 (2016)
10. Karas, M., Glückmann, M., Schäfer, J.: Ionization in matrix-assisted laser desorption/ionization: singly charged molecular ions are the lucky survivors. *J. Mass Spectrom.* **35**, 1–12 (2000)
11. Karas, M., Krüger, R.: Ion formation in MALDI: the cluster ionization mechanism. *Chem. Rev.* **103**, 427–439 (2003)
12. Jaskolla, T.W., Karas, M.: Compelling evidence for lucky survivor and gas phase protonation: the unified MALDI analyte protonation mechanism. *J. Am. Soc. Mass Spectrom.* **22**, 976–988 (2011)
13. Ahn, S.H., Park, K.M., Bae, Y.J., Kim, M.S.: Quantitative reproducibility of mass spectra in matrix-assisted laser desorption ionization and unraveling of the mechanism for gas-phase peptide ion formation. *J. Mass Spectrom.* **48**, 299–305 (2013)
14. Chu, K.Y., Lee, S., Tsai, M., Lu, I., Dyakov, Y.A., Lai, Y.H., Lee, Y., Ni, C.: Thermal proton transfer reactions in ultraviolet matrix-assisted laser desorption/ionization. *J. Am. Soc. Mass Spectrom.* **25**, 310–318 (2014)
15. Lu, I.-C., Chu, K.Y., Lin, C.-Y., Wu, S.-Y., Dyakov, Y.A., Chen, J.-L., Gray-Weale, A., Lee, Y.-T., Ni, C.-K.: Ion-to-neutral ratios and thermal proton transfer in matrix-assisted laser desorption/ionization. *J. Am. Soc. Mass Spectrom.* **26**, 1242–1251 (2015)
16. Ehring, H., Karas, M., Hillenkamp, F.: Role of photoionization and photochemistry in ionization processes of organic molecules and relevance for matrix-assisted laser desorption ionization mass spectrometry. *Org. Mass Spectrom.* **27**, 472–480 (1992)
17. Allwood, D.A., Dreyfus, R.W., Perera, I.K., Dyer, P.E.: UV optical absorption of matrices used for matrix-assisted laser desorption/ionization. *Rapid Commun. Mass Spectrom.* **10**, 1575–1578 (1996)
18. Homeföer, V., Dreisewerd, K., Lüdemann, H.-C., Hillenkamp, F., Läge, M., Strupat, K.: Is the incorporation of analytes into matrix crystals a prerequisite for matrix-assisted laser desorption/ionization mass spectrometry? A study of five positional isomers of dihydroxybenzoic acid. *Int. J. Mass Spectrom.* **185/187**, 859–870 (1999)
19. Chen, X., Carroll, J.A., Beavis, R.C.: Near-ultraviolet-induced matrix-assisted laser desorption/ionization as a function of wavelength. *J. Am. Soc. Mass Spectrom.* **9**, 885–891 (1998)
20. Soltwisch, J., Jaskolla, T.W., Hillenkamp, F., Karas, M., Dreisewerd, K.: Ion yields in UV-MALDI mass spectrometry as a function of excitation laser wavelength and optical and physico-chemical properties of classical and halogen-substituted MALDI matrices. *Anal. Chem.* **84**, 6567–6576 (2012)
21. Soltwisch, J., Jaskolla, T.W., Dreisewerd, K.: Color matters—material ejection and ion yields in UV-MALDI mass spectrometry as a function of laser wavelength and laser fluence. *J. Am. Soc. Mass Spectrom.* **24**, 1477–1488 (2013)
22. Niehaus, M., Schnapp, A., Koch, A., Soltwisch, J., Dreisewerd, K.: New insights into the wavelength dependence of MALDI mass spectrometry. *Anal. Chem.* **89**, 7734–7741 (2017)
23. Tang, K., Taranenko, N.I., Allman, S.L., Chen, C.H., Ch'ang, L.Y., Jacobson, K.B.: Picolinic acid as a matrix for laser mass spectrometry of nucleic acids and proteins. *Rapid Commun. Mass Spectrom.* **8**, 673–677 (1994)
24. Taranenko, N.I., Tang, K., Allman, S.L., Ch'ang, L.Y., Chen, C.H.: 3-Aminopicolinic acid as a matrix for laser desorption mass spectrometry of biopolymers. *Rapid Commun. Mass Spectrom.* **8**, 1001–1006 (1994)
25. Schiller, J., Süß, R., Fuchs, B., Müller, M., Petković, M., Zschörnig, O., Waschipky, H.: The suitability of different DHB isomers as matrices for the MALDI-TOF MS analysis of phospholipids: which isomer for what purpose? *Eur. Biophys. J.* **36**, 517–527 (2007)
26. Mccarley, T.D., Mccarley, R.L., Limbach, P.A.: Electron-transfer ionization in matrix-assisted laser desorption/ionization mass spectrometry. *Anal. Chem.* **70**, 4376–4379 (1998)
27. Karas, M., Bachmann, D., Hillenkamp, F.: Influence of the wavelength in high-irradiance ultraviolet laser desorption mass spectrometry of organic molecules. *Anal. Chem.* **57**, 2935–2939 (1985)
28. Strupat, K., Karas, M., Hillenkamp, F.: 2,5-Dihydroxybenzoic acid: a new matrix for laser desorption-ionization mass spectrometry. *Int. J. Mass Spectrom. Ion Processes.* **111**, 89–102 (1991)
29. Luo, G., Marginean, I., Vertes, A.: Internal energy of ions generated by matrix-assisted laser desorption/ionization. *Anal. Chem.* **74**, 6185–6190 (2002)
30. Boekelmann, V., Spengler, B., Kaufmann, R.: Dynamical parameters of ion ejection and ion formation in matrix-assisted laser desorption/ionization. *Eur. Mass Spectrom.* **1**, 81–93 (1995)
31. Heise, T.W., Yeung, E.S.: Dynamics of matrix-assisted laser desorption as revealed by the associated acoustic signal. *Anal. Chim. Acta.* **299**, 377–385 (1995)
32. Wiegelmann, M., Soltwisch, J., Jaskolla, T.W., Dreisewerd, K.: Matching the laser wavelength to the absorption properties of matrices increases the ion yield in UV-MALDI mass spectrometry. *Anal. Bioanal. Chem.* **405**, 6925–6932 (2013)
33. Allwood, D.A., Dreyfus, R.W., Perera, I.K., Dyer, P.E.: Optical absorption of matrix compounds for laser-induced desorption and ionization (MALDI). *Appl. Surf. Sci.* **109/110**, 154–157 (1997)
34. Dreisewerd, K.: The desorption process in MALDI. *Chem. Rev.* **103**, 395–426 (2003)
35. Westmacott, G., Ens, W., Hillenkamp, F., Dreisewerd, K., Schürenberg, M.: The influence of laser fluence on ion yield in matrix-assisted laser desorption ionization mass spectrometry. *Int. J. Mass Spectrom.* **221**, 67–81 (2002)
36. Dreisewerd, K., Schürenberg, M., Karas, M., Hillenkamp, F.: Influence of the laser intensity and spot size on the desorption of molecules and ions in matrix-assisted laser desorption/ionization with a uniform beam profile. *Int. J. Mass Spectrom. Ion Processes.* **141**, 127–148 (1995)
37. Qiao, H., Spicer, V., Ens, W.: The effect of laser profile, fluence, and spot size on sensitivity in orthogonal-injection matrix-assisted laser desorption/ionization time-of-flight mass spectrometry. *Rapid Commun. Mass Spectrom.* **22**, 2779–2790 (2008)
38. Soltwisch, J., Jaskolla, T.W., Dreisewerd, K.: Erratum to: Color matters—material ejection and ion yields in UV-MALDI mass spectrometry as a function of laser wavelength and laser fluence. *J. Am. Soc. Mass Spectrom.* **26**, 1641–1641 (2015)
39. Hsieh, Y., Casale, R., Fukuda, E., Chen, J., Knemeyer, I., Wingate, J., Morrison, R., Korfmacher, W.: Matrix-assisted laser desorption/ionization imaging mass spectrometry for direct measurement of clozapine in rat brain tissue. *Rapid Commun. Mass Spectrom.* **20**, 965–972 (2006)
40. Tsai, M.T., Lee, S., Lu, I.C., Chu, K.Y., Liang, C.W., Lee, C.H., Lee, Y.T., Ni, C.K.: Ion-to-neutral ratio of 2,5-dihydroxybenzoic acid in matrix-assisted laser desorption/ionization. *Rapid Commun. Mass Spectrom.* **27**, 955–963 (2013)
41. Steven, R.T., Race, A.M., Bunch, J.: Probing the relationship between detected ion intensity, laser fluence, and beam profile in thin film and tissue in MALDI MSI. *J. Am. Soc. Mass Spectrom.* **27**, 1419–1428 (2016)
42. Donegan, M., Tomlinson, A.J., Nair, H., Juhasz, P.: Controlling matrix suppression for matrix-assisted laser desorption/ionization analysis of small molecules. *Rapid Commun. Mass Spectrom.* **18**, 1885–1888 (2004)
43. Martic, S., Brennan, J.D., Brook, M.A., Ackloo, S., Nagy, N.: Towards the development of a covalently tethered MALDI system—a study of allyl-modified MALDI matrices. *Can. J. Chem.* **85**, 66–76 (2007)
44. Westman, A., Huth-Fehre, T., Demirev, P., Bielawski, J., Medina, N., Sundqvist, B.U.R., Karas, M.: Matrix-assisted laser desorption/ionization: dependence of the ion yield on the laser beam incidence angle. *Rapid Commun. Mass Spectrom.* **8**, 388–393 (1994)
45. Tambe, S., Blott, H., Fülöp, A., Spang, N., Flottmann, D., Bräse, S., Hopf, C., Junker, H.D.: Structure-performance relationships of phenyl cinnamic acid derivatives as MALDI-MS matrices for sulfatide detection. *Anal. Bioanal. Chem.* **409**, 1569–1580 (2017)
46. Rheims, J., Köser, J., Wriedt, T.: Refractive-index measurements in the near-IR using an Abbe refractometer. *Meas. Sci. Technol.* **8**, 601–605 (1999)
47. Kedenburg, S., Vieweg, M., Gissibl, T., Giessen, H.: Linear refractive index and absorption measurements of nonlinear optical liquids in the visible and near-infrared spectral region. *Opt. Mater. Express.* **2**, 1588 (2012)
48. Steven, R.T., Dexter, A., Bunch, J.: Investigating MALDI MSI parameters (Part 2) – On the use of a mechanically shuttered trigger system for improved laser energy stability. *Methods.* **104**, 111–117 (2016)

49. Steven, R.T., Palmer, A.D., Bunch, J.: Fluorometric beam profiling of UV MALDI lasers. *J. Am. Soc. Mass Spectrom.* **24**, 1146–1152 (2013)
50. Schneider, C.A., Rasband, W.S., Eliceiri, K.W.: NIH Image to ImageJ: 25 years of image analysis. *Nat. Methods.* **9**, 671–675 (2012)
51. Race, A.M., Styles, I.B., Bunch, J.: Inclusive sharing of mass spectrometry imaging data requires a converter for all. *J. Proteom.* **75**, 5111–5112 (2012)
52. Race, A.M., Palmer, A.D., Dexter, A., Steven, R.T., Styles, I.B., Bunch, J.: SpectralAnalysis: software for the masses. *Anal. Chem.* **88**, 9451–9458 (2016)
53. Schwoerer, M., Wolf, H.C.: Organic molecular solids. Wiley-VCH Verlag GmbH, Weinheim, (2006)
54. Reichardt, C., Welton, T.: Solvents and solvent effects in organic chemistry. Wiley-VCH Verlag GmbH & Co. KGaA, Weinheim (2010)
55. Flakus, H.T., Miros, A., Jones, P.G.: Influence of molecular electronic properties on the IR spectra of dimeric hydrogen bond systems: polarized spectra of 2-hydroxybenzothiazole and 2-mercaptobenzothiazole crystals. *J. Mol. Struct.* **604**, 29–44 (2002)
56. Tanaka, J.: The electronic spectra of aromatic molecular crystals. I. Substituted benzene molecules. *Bull. Chem. Soc. Jpn.* **36**, 833–847 (1963)
57. Karas, M., Bahr, U., Strupat, K., Hillenkamp, F., Tsarboboulos, A., Pramanik, B.N.: Matrix dependence of metastable fragmentation of glycoproteins in MALDI TOF mass spectrometry. *Anal. Chem.* **67**, 675–679 (1995)
58. Stübiger, G., Belgacem, O.: Analysis of lipids using 2,4,6-trihydroxyacetophenone as a matrix for MALDI Mass Spectrometry. *Anal. Chem.* **79**, 3206–3213 (2007)
59. Guenther, S., Koestler, M., Schulz, O., Spengler, B.: Laser spot size and laser power dependence of ion formation in high resolution MALDI imaging. *Int. J. Mass Spectrom.* **294**, 7–15 (2010)
60. Liu, B., Charkin, O.P., Klemenko, N., Chen, C.W., Wang, Y.: Initial ionization reaction in matrix-assisted laser desorption/ionization. *J. Phys. Chem. B.* **114**, 10853–10859 (2010)
61. Wiegelmann, M., Dreisewerd, K., Soltwisch, J.: Influence of the laser spot size, focal beam profile, and tissue type on the lipid signals obtained by MALDI-MS imaging in oversampling mode. *J. Am. Soc. Mass Spectrom.* **27**, 1952–1964 (2016)
62. Sadeghi, M., Vertes, A.: Crystallite size dependence of volatilization in matrix-assisted laser desorption ionization. *Appl. Surf. Sci.* **127/129**, 226–234 (1998)
63. Ehring, H., Sundqvist, B.U.R.: Studies of the MALDI process by luminescence spectroscopy. *J. Mass Spectrom.* **30**, 1303–1310 (1995)
64. Allwood, D., Dyer, P.: Quantitative fluorescence measurements performed on typical matrix molecules in matrix-assisted laser desorption/ionisation. *Chem. Phys.* **261**, 457–467 (2000)
65. Price, D.M., Bashir, S., Derrick, P.R.: Sublimation properties of x,y-dihydroxybenzoic acid isomers as model matrix assisted laser desorption ionization (MALDI) matrices. *Thermochim. Acta.* **327**, 167–171 (1999)
66. Roux, M.V., Temprado, M., Jiménez, P., Foces-Foces, C., Notario, R., Parameswar, A.R., Demchenko, A.V., Chickos, J.S., Deakynne, C.A., Liebman, J.F.: Experimental and theoretical study of the structures and enthalpies of formation of 3 H -1,3-benzoxazole-2-thione, 3 h -1,3-benzothiazole-2-thione, and their tautomers. *J. Phys. Chem. A.* **114**, 6336–6341 (2010)
67. Monte, M.J.S., Gonçalves, M.V., Ribeiro Da Silva, M.D.M.C.: Vapor pressures and enthalpies of combustion of the dihydroxybenzoic acid isomers. *J. Chem. Eng. Data.* **55**, 2246–2251 (2010)
68. Astigarraga, E., Barreda-Gómez, G., Lombardero, L., Fresnedo, O., Castaño, F., Giralt, M.T., Ochoa, B., Rodríguez-Puertas, R., Fernández, J.A.: Profiling and imaging of lipids on brain and liver tissue by matrix-assisted laser desorption/ionization mass spectrometry using 2-mercaptobenzothiazole as a matrix. *Anal. Chem.* **80**, 9105–9114 (2008)
69. Steven, R.T., Race, A.M., Bunch, J.: Para-nitroaniline is a promising matrix for MALDI-MS imaging on intermediate pressure MS systems. *J. Am. Soc. Mass Spectrom.* **24**, 801–804 (2013)